Density Functional Study of the Radical Reactions of 3-Methyl-1-phenyl-2-pyrazolin-5-one (MCI-186): Implication for the Biological Function of MCI-186 as a Highly Potent Antioxidative Radical Scavenger

Satoshi Ono,[†,‡] Keiji Okazaki,[†] Minoru Sakurai,[*,‡] and Yoshio Inoue[‡]

Yokohama Research Center, Mitsubishi Chemical Corporation, 1000, Kamoshida-cho, Aoba-ku, Yokohama 227, Japan, and Department of Biomolecular Engineering, Tokyo Institute of Technology, 4259, Nagatsuta-cho, Midori-ku, Yokohama 226, Japan

Received: October 21, 1996; In Final Form: January 22, 1997[⊗]

The radical reaction intermediates and products from the antioxidative radical scavenger MCI-186, 3-methyl-1-phenyl-2-pyrazolin-5-one (**1**), and its model system 1,3-dimethyl-2-pyrazolin-5-one (**2**) are investigated by a density functional method (B3LYP/6-31G*) with the self-consistent isodensity polarized continuum model (SCI-PCM). It is shown that a radical intermediate, denoted **4**, is produced as a result of one-electron oxidation of **2** by active oxygen species. The subsequent reactions are studied along the scheme proposed previously by an *in vitro* experimental study of **1**. For **4**, the isotropic hyperfine coupling constants are calculated using the B3LYP/EPR-II basis set, and the results are compared with the literature values given by ESR measurements at room and body temperatures. Consequently, it is confirmed that the calculation reproduces well the experimental results. One of the most important findings is that the radical intermediate is stabilized by delocalization of spin population over the pyrazoline ring and the oxygen atom. In addition, it is of great interest that the hydrogen attached to the C4 carbon of **4** exhibits the nature of an exchangeable proton. As a result of this, at least in the aqueous medium **4** should be equilibrated with its anionic form **4′** . **4′** is shown to have a more delocalized spin population than **4**. Due to such spin delocalization, the radical intermediates **4** and **4′** have less ability of peroxidizing lipid molecules than typical active oxygen species, such as •OH or LOO•. This directly accounts for the antioxidative activity of **1** and **2**. Finally, the reactions of **1** that would occur in the lipid phase will be discussed on the basis of the present calculated results.

Introduction

Lipid peroxidation caused by active oxygen species plays an important role in the development of brain edema and tissue injury in ischemic and postischemic damages.[1,2] MCI-186, 3-methyl-1-phenyl-2-pyrazolin-5-one (**1**), shows highly advantageous effects on several brain ischemic models.[3−5] For example, an intravenous injection of **1** strongly attenuated ischemic and postischemic brain edema induced by the occlusion of the middle cerebral artery of rats.[3] Preischemic treatment with **1** prevented brain edema and the changes in concentrations of sodium and potassium ions in the brain, induced by hemispheric embolization of rat brains.[4] Preischemic treatment with **1** also facilitated the recovery of electrocorticographic activity and prolonged survival time in global complete ischemia of rats. Furthermore, postischemic treatment decreased cortical infarction in focal embolization of rats.[5] The anti-ischemic action of **1** has been ascribed to its activity as an antioxidative radical scavenger. However, it remains unclear how **1** reacts with active oxygen species and why it exhibits antioxidative activity. Therefore, it is necessary to provide unambiguous answers to such questions.

1 has three tautomeric forms, **1a**, **1b**, and **1c** (see Figure 1), and the nature of this tautomeric equilibrium has been studied extensively in various solvents by means of many experimental methods such as ^{1}H-NMR, ^{13}C-NMR, ^{15}N-NMR, UV, IR, and X-ray.[6−8] On the other hand, it has been indicated that the density functional theory provides good insight into the tautomerism of various heterocyclic molecules, such as 2-pyridone/2-hydroxypyridine,[9] protonated cycosine,[10] some five- and six-membered nitrogen heterocyclics,[11] adenine[12] and 5-nitro-2,4-dihydro-3*H*-1,2,4-triazolone.[13] We have already investigated the tautomeric equilibria of 3-methyl-(1-substituted)-2-pyrazolin-5-one including **1** in the gaseous and aqueous phases using the density functional theory.[14]

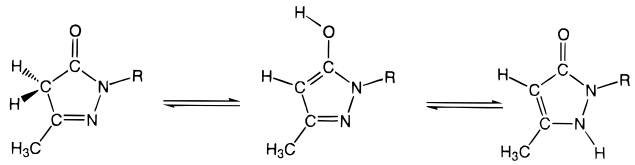

1 : R=C_6H_5
2 : R=CH_3

Figure 1. Tautomeric equilibrium of 3-methyl-1-phenyl-2-pyrazolin-5-one (**1**) and 1,3-dimethyl-2-pyrazolin-5-one (**2**).

Here we focus on the mechanism of the radical reaction of **1**. Intermediate radical species produced from **1** were detected by ESR in deoxygenate solutions.[15,16] The subsequent reaction has been investigated by various analytical methods. Recently, Yamamoto et al.[17] reported the reaction between **1** and peroxyl radicals produced from azo initiators and proposed a reaction scheme shown in Figure 2. Anionic form **1′** is converted more effectively with peroxyl radical than nonionic form **1**, and 3-methyl-1-phenyl-2-pyrazolin-4,5-dione (**5**) is formed from the radical reaction, which is subsequently hydrolyzed to the final product, 2-oxo-3-(phenylhydrazono)butanoic acid (**6**). A minor product is 4-hydroxy-4-(3-methyl-1-phenyl-1*H*-pyrazolin-5-on-4-yl)-3-methyl-1-phenyl-1*H*-pyrazolin-5-one (**7**). They also

* Author to whom all correspondence should be addressed.
† Mitsubishi Chemical Corporation.
‡ Tokyo Institute of Technology.
⊗ Abstract published in *Advance ACS Abstracts,* May 1, 1997.

S1089-5639(96)03267-7 CCC: $14.00

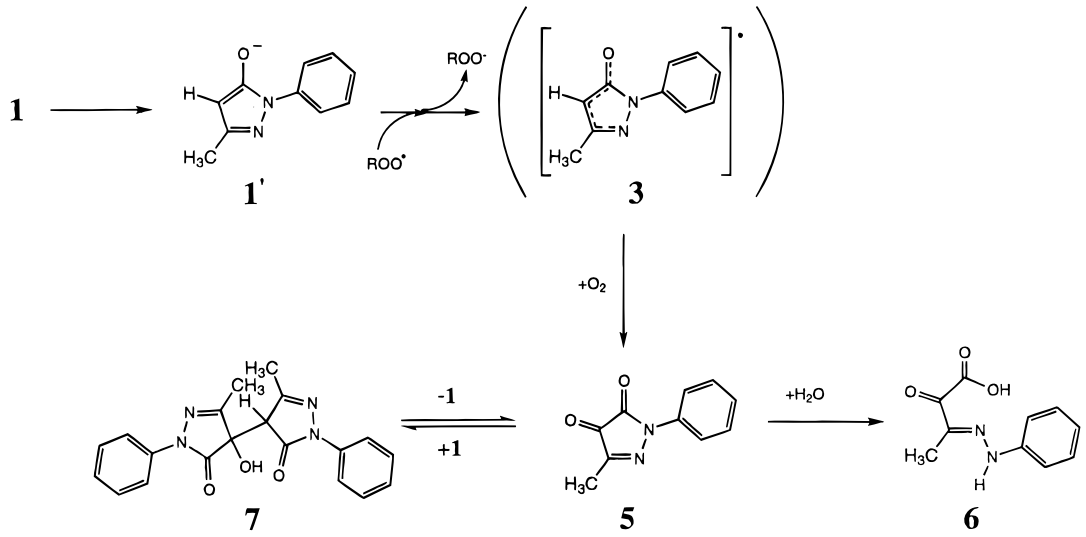

Figure 2. Hypothetical reaction mechanism of **1** based on an *in vitro* experimental study (ref 17).

showed that **1** inhibits the oxidation of unilamellar soybean phosphatidylcholine liposome, a reaction which is initiated by both water-soluble and lipid-soluble radical initiators. No stable radical recombination products were found.

In this work, three main subjects are dealt with theoretically. (1) What is the main radical intermediate produced from **1**? (2) Why is **1** able to inhibit lipid peroxidation? and (3) How stable are the major products? Combining these results with available experimental data, we will reveal the physical origin of the antioxidative activity of **1**.

For the medium size molecules such as MCI-186, we may expect a faster throughput by using semiempirical methods, or the use of Hartree−Fock calculations to get more accurate results than the semiempirical ones. However, the wave functions obtained from these methods may involve a large quantity of spin contamination. Here, we adopt a density functional method, which enables us to avoid the artifacts from spin contamination and to save CPU time.

Computational Method

Density functional calculations (DFT) were performed using the Gaussian 94 program[18] on RS/6000 SP2 and Cray C916/12256 systems. Full geometry optimizations were carried out with the 6−31G* basis set[19] at the Becke3LYP (hereafter denoted as B3LYP)[20] level with $\epsilon = 1.0$ (gas phase) and $\epsilon = 78.3$ (aqueous phase). Radical states were calculated by unrestricted B3LYP. The solute−solvent interaction was taken into account by the self-consistent isodensity polarized continuum model (SCI-PCM) with dielectric constant $\epsilon = 78.3$. In this method, the cavity surface is formed by an envelope of isodensity surfaces, on which electron density is 0.0004 au. The default method of numerical surface integration given in the program is based on a Lebedev type grid (75,302) generated around each atomic center. However, when the method was applied to medium size molecules studied here, the SCF cycles often failed to converge. Instead of the multicentered grid, we adopted a single-centered grid, where the origin was placed at the molecular center of gravity and 800 grid points were formed with $(\psi,\phi) = (40,20)$. For comparison, some test calculations were performed using the default method, the single-centered (40,20), and the single-centered (60,40). There were only slight differences (<0.03 kcal/mol) in energy among them, and the dipole moment and the energy level of the HOMO were also identical with each other within 1%. Among the three methods, the single-centered (40,20) is the most favorable in CPU time. Thus, we believe that this is a better method for grid formation of medium size molecules.

To evaluate the effects of explicit hydrogen bondings with water molecules, we also evaluated the solvent−solute interactions by the hydrogen-bonded complex for radical **4** with three explicit water molecules, which have hydrogen bonds with oxygen and nitrogen atoms of **4**. The geometry is fully optimized with B3LYP/6-31G*.

ESR isotropic hyperfine coupling constants a_N calculation was performed using the EPR-II basis set,[21−26] after the molecular geometries were fully optimized by using the same basis set. The EPR-II basis set was called DZP′ in previous papers by Barone et al.,[22−25] since it is based on the Huzinaga−Dunning polarized double-ζ basis set (DZP). In the EPR-II, the outer core−inner valence region of heavy atoms is uncontracted and a very tight s function is newly, added to hydrogen: namely, this basis set is expressed by (3,1,1/1) for hydrogen and (5,1,1,1,1/4,1) for the second-row atoms. The EPR-II basis set has been used to calculate ESR parameters of various radicals, including σ radicals,[22] fluorovinyl radicals,[23] carbon-centered π radicals,[24] Schiff base radicals,[24] small organic radicals,[25] and dihydronitrosyl radicals.[26] Adamo et al. compared the results from the EPR-II basis set with those from a larger basis set called TZ2P′ and stated that for the computation of EPR parameters the cheaper DZP′ (EPR-II) basis set appears sufficient.[24]

The isotropic hyperfine coupling constants was derived from the following formula:

$$a_{\mathrm{N}}(\mathrm{iso}) = \frac{8}{3}\pi g_{\mathrm{e}} g_{\mathrm{N}} \beta \beta_{\mathrm{N}} \rho(r_{\mathrm{N}})$$

where g_e, g_N are the electron and nuclear magnetogyric ratios, β, β_N are the electron and nuclear magnetons, and $\rho(r_N)$ is the Fermi contact term.

We evaluated the accuracy of the B3LYP/EPR-II basis set for radicals generated from a nitrogen-containing heterocyclic of some azolinones in the gaseous and aqueous phases, by comparing the calculated results with the experimental results reported by Shohoji et al.[27] For comparison, some calculations using B3LYP/6-31G* were also performed. The results showed that the 6-31G* calculation tends to overestimate the isotropic hyperfine coupling constants, but the EPR-II results tend to slightly underestimate it. It was found that the incorporation of solvent effects improves the accuracy of predicting isotropic

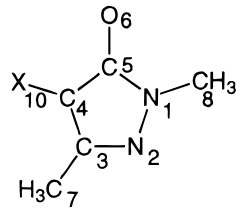

Figure 3. Numbering notation of **2** and its derivatives.

hyperfine coupling constants. It is thus reasonable to say that the EPR-II is useful for predicting the electronic states of the heterocyclic radicals studied here. The details of these results will be published elsewhere.[28]

Results and Discussion

It is known that **1** inhibits the lipid oxidation initiated by water-soluble and lipid-soluble radical initiators.[17] This fact indicates that **1** could be distributed between the aqueous and lipid phases and thereby prevent the lipid peroxidation in both phases. To take into account both situations, two different environments were assumed in the SCI-PCM calculations: in the first case dielectric constant ϵ was taken to be 78.3, and in the second ϵ was taken to be 1.0, corresponding to the aqueous and gas phases, respectively. The acyl lipid chain is similar to a normal alkane in polarity, and thereby the dielectric constant of the hydrophobic region of the lipid bilayer would be about 2. Here, the reactions that would occur in the lipid phase will be estimated from the calculated results for the gas and aqueous phases.

The DFT calculation described above was applied mainly to a model system of **1**, 1,3-dimethyl-2-pyrazolin-5-one (**2**), in which the phenyl ring of **1** is replaced by the methyl group. It will be discussed below that such a structural truncation hardly influences the main conclusion drawn in this study. The numbering notation of **2** and its derivatives is shown in Figure 3. The reaction scheme expected for **2** is shown in Figure 4, which is equivalent to Figure 2. Calculations were performed along the reaction schemes shown in Figure 4 and Figure 5. The optimized geometries obtained at the B3LYP/6-31G* level of calculation are listed in Table 1 The energy change accompanied by each reaction is listed in Table 2.

Anionic Form. Oxidation of **1**, initiated by a radical initiator, depends on the pH of buffer solution.[17] When the pH is larger than 7.0, the reaction proceeds effectively. Since the pK_a of **1** is 7.0,[17] this fact suggests that the anionic form of **1** is more reactive than the nonionic form **1**. Similar pH dependence has been also reported on the reaction between 4-methyl-2-pyrazolin-5-one and the bromine anion radical.[29]

As can be seen from Table 2, the energy change accompanied by the following reaction is -37.12 kcal mol^{-1} in the aqueous phase: **2a** + $OH^- \rightarrow$ **2′** + H_2O. This finding indicates that in basic aqueous solution **2′** is more stable than **2a**, consistent with the above experimental result. According to the B3LYP/6-31G* calculation, **2a** had the lowest ground state energy among the three tautomers (Figure 1) in both the aqueous and gaseous phases. Hereafter, our main attention will be given only to **2a**.

To examine the reason why the anionic form is more reactive than the nonionic one, the energies of the HOMO's were compared between **2** and **2′**. In the aqueous solution, the HOMO level of the anionic form **2′** was -0.126 au, and that of each tautomer (see Figure 1; **2a**, **2b**, and **2c**) of **2** was between -0.206 and -0.221.[14] A higher HOMO level may indicate a better electron donor, consequently facilitating a reaction with the SOMO of a radical. Thus, the calculation indicates that the anionic form **2′** is more easily oxidized by a radical, such as the peroxyl radical LOO•, generating **4** and LOO^-. This is again consistent with the experimental results of reactions from **1** to **3** in Figure 2.[17]

Radical States. Lehmann et al.[15] observed ESR spectra of radical state **3** at body temperature in deoxygenate aqueous buffer. Omelka et al.[16] measured the corresponding spectra at room temperature in deoxygenate benzene. Both results showed that the isotropic hyperfine coupling constants are detectable only at N2, that is, a_N (N2), and its value is 0.67 mT. In addition, the lifetime of the radical was estimated to be 2−3 min. According to these results, it is reasonable to assume that at room temperature H10 attached to C4 of a radical intermediate **3** is rapidly exchanged with exchangeable protons of solvent or with those of neighboring radical molecules.

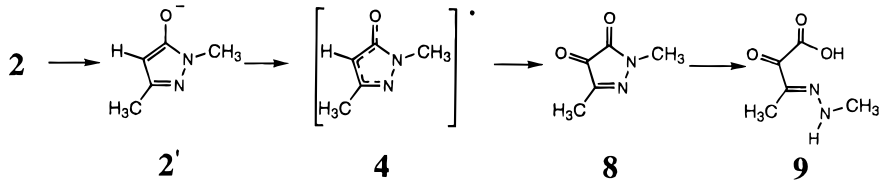

Figure 4. Reactions of model compound **2**. In this scheme, it is assumed that **2** would undergo reactions similar to Figure 2 found for **1**.

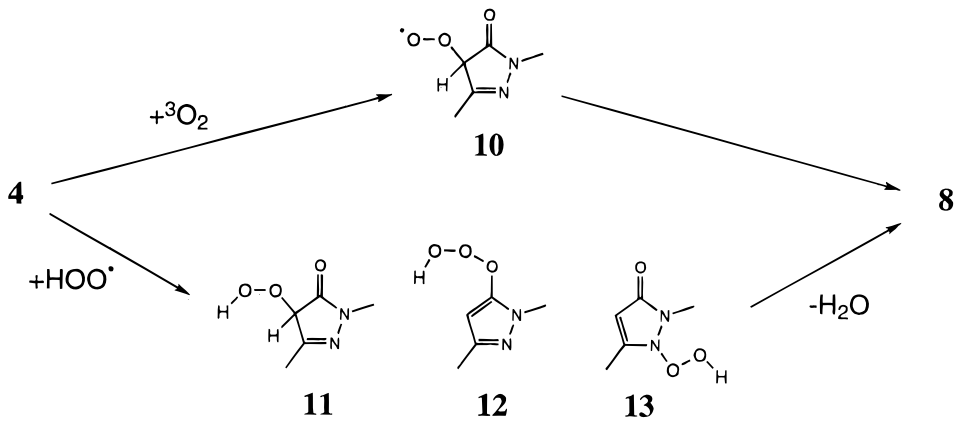

Figure 5. Two possible reactions on going from **4** to **8**. One type of reaction assumes the addition of an oxygen molecule to **4**, producing the radical intermediate **10**. The other assumes the addition of peroxyl radical to **4**, producing three types of adducts **11**, **12**, and **13**.

TABLE 1: Optimized Geometries Obtained at the B3LYP/6-31G* Level[a]

	2′		**4**		**4′**		**8**	
	$\epsilon = 1.0$	$\epsilon = 78.3$	$\epsilon = 1.0$	$\epsilon = 78.3$	$\epsilon = 1.0$	$\epsilon = 78.3$	$\epsilon = 1.0$	$\epsilon = 78.3$
N1−N2	1.387	1.386	1.325	1.325	1.351	1.346	1.396	1.403
N2−C3	1.337	1.338	1.385	1.388	1.375	1.378	1.296	1.295
C3−C4	1.407	1.407	1.372	1.371	1.410	1.407	1.488	1.489
C4−C5	1.429	1.425	1.451	1.450	1.479	1.477	1.557	1.556
C5−N1	1.411	1.402	1.426	1.423	1.440	1.428	1.372	1.361
C5−O6	1.260	1.269	1.231	1.234	1.246	1.251	1.209	1.210
C3−C7	1.507	1.506	1.496	1.495	1.510	1.510	1.215	1.220
C4−H10(O10)	1.083	1.083	1.080	1.080			1.495	1.490
N1−C8	1.428	1.436	1.449	1.452	1.433	1.442	1.447	1.449
N1−N2−C3	103.0	103.6	106.1	106.3	104.0	104.6	110.1	110.2
N2−C3−C4	113.4	112.8	111.4	111.2	117.7	116.9	110.3	109.9
C3−C4−C5	106.8	106.7	106.6	106.5	99.4	99.5	103.3	103.4
C4−C5−N1	102.2	102.8	103.1	103.5	107.8	108.3	102.8	103.2
C5−N1−N2	114.6	114.1	112.8	112.6	111.2	110.8	113.5	113.3
C4−C5−O6	134.5	133.7	133.3	132.9	132.8	131.5	128.8	127.8
N2−C3−C7	119.5	120.0	118.7	118.8	116.5	116.2	124.3	123.9
N2−N1−C8	121.2	120.6	122.0	121.9	122.1	121.7	119.5	119.1
N1−N2−C5−C8	0.0	0.0	0.0	0.0	0.0	−0.1	0.0	0.1
N1−N2−C3−C4	0.0	0.0	0.0	0.0	0.0	−0.0	0.0	0.0
N2−C3−C4−C5	0.0	0.0	0.0	0.0	0.0	0.00	0.0	0.0
H10−C4−C5−C3	180.0	180.0	180.0	180.0				

[a] The bond lengths are in angstroms, angles and torsion angles are in degrees.

TABLE 2: Energy Change (ΔE) Accompanied by Some Radical Reactions Obtained by the B3LYP/6-31G* [a]

			ΔE/kcal mol^{-1}	
			gas phase	$\epsilon = 78.3$
2a + OH^-	→	**2′** + H_2O	−67.38	−37.12
2a + •OH	→	**4** + H_2O	−34.95	−35.21
4 + $^3O_2$	→	**10**	−1.38	−3.74
4 + •OOH	→	**11**	−40.14	−36.71
		12	+9.37	+12.04
		13	−14.93	−12.92
11	→	**8** + H_2O	−41.53	−47.96
8 + H_2O	→	**9**	−13.90	−11.60

[a] ΔE in kcal mol^{-1}.

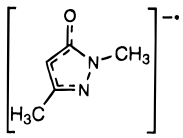

4′

Figure 6. Molecular structure of anionic radical **4′**. Its presence is assumed from the fact that H10 of **4** is an exchangeable proton.

At low temperatures, the isotropic hyperfine coupling constants can be observed at both positions of N2 and H10, because such an exchange becomes less important. Sevilla et al.[30] measured ESR spectra of an analog of **1**, 3-methyl-1-[2-(2-napthyloxy)-ethyl]-2-pyrazolin-5-one (Nafazatrom), at 77 K in the $NaClO_4$ matrix with UV irradiation. As a result, a_N (N2) and a_N (H10) were determined to be 0.7 and 0.6 mT, respectively. According to these experimental results, we took into account two kinds of species, **4** and **4′** (See Figure 6), as the radical intermediates produced from **2**.

In the B3LYP/6−31G* level of calculation, the degree of spin contamination of **4** and **4′** was estimated to be $0.765 < \langle S^2 \rangle < 0.772$. By annihilation of the quartet contribution, $\langle S^2 \rangle$ became 0.7502, indicating no residual spin contamination. Consequently, the B3LYP/6−31G* method can be safely used for the calculation of structures and spin-dependent properties of **4** and **4′**. The structures and energies of **4** and **4′** are shown in Table 1 and Table 3. These radicals are planar because they are conjugated systems.

The calculated isotropic hyperfine coupling constants obtained from the B3LYP/EPR-II calculation are listed in Table 4 and Table 5. For **4** in the aqueous phase, the isotropic hyperfine coupling constants at N2 and H10 were determined as follows: a_N (N2) = 0.551 mT and a_N (H10) = −0.541 mT. For **4′**, a_N (N2) was 0.611 mT. The a_N(N2) value of **4′** is in agreement with the a_N(N2) value for **3** observed at room temperature. However, the calculated data for **4** cannot be compared straightforwardly with the results from the low-temperature experiments mentioned above, because routine ESR measurements do not indicate us the sign of the isotropic hyperfine coupling constants. Only the comparison of the absolute values is meaningful between the calculated and experimental data. In this regard, the calculation well reproduces the hyperfine coupling constants for both N2 and H10 observed at the low temperature.

On the basis of these results, it can be concluded that the present DFT results for **4** are applicable to interpreting the electronic structure of heterocyclic radicals **3**. Table 6 shows the spin population of **4** and **4′**. N2, C4, and O6 have large values of spin population, suggesting that these atomic positions can be regarded as reaction sites. One of the most important findings is that the spin population of both **4** and **4′** is highly delocalized over the pyrazoline ring and the oxygen atom. This is consistent with the ESR results given by Sevilla et al.,[30] who indicated that the above-mentioned analog of **4** (Nafazatrom) has a delocalized spin population.

Furthermore, the SOMO level of the radical was examined, because it is also an indicator of reactivity. The data are listed in Table 7. •OH has the lowest SOMO energy (−0.324 au) among the species studied here and thereby is the most reactive radical. As a model of LOO•, some examples of ROO• (R = Me, Et, Pr, Bu) were computed. The SOMO levels of these radicals were typically −0.274 au, and thereby these radicals may exhibit relatively lower reactivity than •OH. The SOMO level of **4** was −0.216 au, which is the highest value among the radicals studied. It can be thus concluded that **4** and probably **4′** may exhibit less reactivity than typical active oxygen species.

To evaluate the effects of explicit hydrogen bondings with water molecules on the spin populations, a hydrogen-bonded complex was calculated with **4** and three water molecules. While

TABLE 3: Energies, Dipole Moments, $\langle S^2 \rangle$, SOMO Levels, and Zero-Point Energies (ZPE) of 4, 4′ Obtained at the UB3LYP/6-31G* Level[a]

	4		**4′**	
	$\epsilon = 1.0$	$\epsilon = 78.3$	$\epsilon = 1.0$	$\epsilon = 78.3$
energy	−379.433080	−379.439576	−378.7862647	−378.8691159
dipole moment	1.9842	2.5643	4.8662	6.4794
$\langle S^2 \rangle$	0.7668	0.7653	0.7722	0.7714
SOMO	−0.21829	−0.21553	0.01248	−0.14205
ZPE	74.32	74.27	65.39	64.80

[a] Energies and SOMO levels in atomic units, dipole moments in debyes, and ZPE in kcal mol^{-1}.

TABLE 4: Isotropic Hyperfine Coupling Constants of 4 Obtained by the UB3LYP/6-31G* and UB3LYP/EPR-II Levels[a]

	4 (gas phase)		**4** ($\epsilon = 78.3$)		Nafazatrom exptl[b]
	6-31G*	EPR-II	6-31G*	EPR-II	
N2	0.736	0.546	0.744	0.551	0.7
H10	−0.634	−0.576	−0.599	−0.541	0.6

[a] Isotropic hyperfine coupling constants are in milliteslas. [b] From ref 30.

TABLE 5: Isotropic Hyperfine Coupling Constants of 4′ Obtained at the UB3LYP/6-31G* and UB3LYP/EPR-II Levels[a]

	4′ (gas phase)		**4′** ($\epsilon = 78.3$)		
	6-31G*	EPR-II	6-31G*	EPR-II	3′ exptl[b]
N2	0.797	0.620	0.792	0.611	0.67

[a] Isotropic hyperfine coupling constants are in milliteslas. [b] From ref 15 and 16.

TABLE 6: Total Atomic Spin Populations of 4, 4′, and the Hydrogen-Bonded Complex Obtained at the B3LYP/6-31G* Level

	4		**4′**		H-bonded complex[a]
	$\epsilon = 1.0$	$\epsilon = 78.3$	$\epsilon = 1.0$	$\epsilon = 78.3$	$\epsilon = 1.0$
N1	0.112	0.108	0.016	0.189	0.102
N2	0.419	0.425	0.445	0.447	0.428
C3	−0.095	−0.088	−0.173	−0.174	−0.093
C4	0.256	0.237	0.375	0.355	0.231
C5	−0.013	0.011	0.050	0.068	0.040
O6	0.330	0.314	0.286	0.286	0.304
C7	0.007	0.006	0.012	0.011	0.007
H10	−0.012	−0.011			−0.010

[a] See Figure 7.

TABLE 7: Comparison of the SOMO Levels of Some Representative Radicals with Those of 4 and 10[a]

	SOMO/au	
	gas phase	$\epsilon = 78.3$
•OH	−0.329	−0.324
•OOH	−0.292	−0.286
MeO•	−0.282	−0.280
MeOO•	−0.277	−0.278
EtOO•	−0.271	−0.274
PrOO•	−0.270	−0.274
BuOO•	−0.269	−0.273
10	−0.247	−0.247
4	−0.218	−0.216

[a] Obtained by the B3LYP/6-31G* calculation.

there exist many possible orientations for hydrogen-bonded water molecules, we evaluated only one orientation as a test case. The calculated spin populations are listed in Table 6, and Figure 7 shows the orientation of water molecules. It was found that the spin populations of the hydrogen-bonded complex and the SCI-PCM are essentially the same. This suggests that hydrogen bonding has little effect on the spin populations.

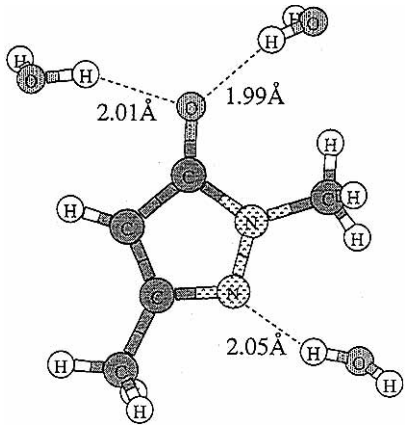

Figure 7. Hydrogen-bonded complex composed of **4** and three water molecules.

As described above, **2** is a model of **1** (MCI-186). To evaluate effects of the structural truncation, we calculated the radical state **3** with full atomic representation (results not shown). It was found that there are no significant differences between **3** and **4**, with respect to the spin populations over the pyrazoline ring and the oxygen atom. This again indicates that structure **2** and its derivatives are good models of structure **1**.

Site of the Oxygen Addition. It can be assumed that the O_2 addition reaction to the intermediate radicals such as **3** and **4** proceeds with zero activation energy.[31] Then, there are three possible reactions sites. Molecular oxygen would attack the N2, C4, or O6 atom of **4** or **4′**, producing N2−OO•, C4−OO•, or O6−OO•, respectively. To examine the relative importance of them, the energy change accompanied by each reaction was evaluated. Consequently, it was indicated that N2−OO• and O6−OO• are spontaneously dissociated, giving molecular oxygen, which means the occurrence of the reverse reaction. According to the present calculation, only the C4−OO• radical (**10**) is shown to exist as a stable adduct. The energy gain in the process of **4** + O_2 → **10** is 3.74 kcal mol^{-1}.

The spin population on the terminal oxygen atom of **10** is 0.4, that on the neighboring oxygen is 0.28, and the residual spins are delocalized on the pyrazoline ring and the O6 oxygen atom. Active oxygen such as •OH has a spin population of 1.0 on the oxygen atom, and that of the terminal oxygen atom in LOO• is 0.7. The SOMO level of **10** was −0.247 au, which is slightly higher than •OH and LOO•. On the basis of these results, radical **10** would also exhibit less reactivity compared to •OH and LOO• radicals. It remains unclear how the radical **10** is converted to **8**.

Site of Peroxyl Radical Addition. Radical recombination products such as **11**, **12**, and **13** have not been detected by *in vitro* experiments for **1**. However, such products may not be negligible as intermediates in the reaction starting from **4** (or from **3**), because they could be easily dehydrolized giving the dione form **8** (or **5**) as well. To investigate this possibility, the calculation was performed for radical recombination products

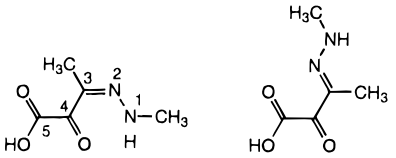

9a **9b**

Figure 8. Stable conformations of **9**. The conformation of **9a** is different from that of **9b** in the rotation of the N2−C3 and C3−C4 bond. The 1−2−3−4 dihedral angles of **9a** and **9b** are 0° and 180°, and 2−3−4−5 of those are 180° and 0°, respectively.

11, **12**, and **13**. As a model of peroxyl radical, we adopt hydroperoxyl radical HOO•. The energy gain on going from **4** + •OOH to these adducts is listed in Table 2. The peroxyl radical is more likely to react with C4 yielding **11**, the energy gain of which is $\Delta E = 36.71$ kcal mol^{-1} in the aqueous phase. Certainly, **11** is easily dehydrated, yielding **8**, where the energy gain is 47.96 kcal mol^{-1}.

Stabilization of the Final Product. According to *in vitro* experiments for **1**, **6** is the final product, which is produced directly by the hydrolysis of **5**.[17] As a model of this reaction, we examined the reaction from **8** to **9**. **9** could take many conformations. Some conformational searches were done by rotating the N2−C3 and C3−C4 bonds. The most stable conformation was found to be **9a** in the aqueous phase, while **9b** was the most stable one in the gas phase (see Figure 8). The energy gain on going from **8** + H_2O to **9** is 11.60 kcal mol^{-1} in the aqueous phase, indicating the preferential formation of **9**.

Features of MCI-186. As described above, the present DFT calculation for **2** and its derivatives reproduces well the available experimental results for the radical reaction of **1** in the aqueous medium. The calculated results provided clear answers to some important problems that could be solved only by conventional experimental techniques.

First, it was revealed the reason that **1** (MCI-186) exhibits highly potent antioxidative activity. This question is represented in another way: why does the radical intermediate **4** (or **3**) exhibit less oxidative activity than active oxygen species such as •OH and LOO•? This is a clue to understanding the biological function of **1**, because *in vivo* **3** is also expected to be the first product generated by the reaction of **1** with active oxygen species occurring after ischemia-reperfusion. According to the present calculation, **4** (equivalent to **3**) has a highly delocalized spin population. This is in contrast to the cases of •OH and LOO•. The spin population of **4** was shown to be distributed mainly on O6, N2, and C4: in the aqueous medium the population values on these atoms were 0.314, 0.425, and 0.237, respectively. On the other hand, the spin populations on the oxygen of •OH and the terminal oxygen of LOO• were 1.0 and 0.7, respectively. Clearly, the reaction sites of **4** have considerably less activity than those of typical active oxygen species. A similar conclusion was also deduced from the fact that **4** has the highest SOMO level among the radicals studied. In the subsequent reactions on going from **4** to **9**, at least one radical intermediate (**10**) would be formed. At present, it remains to be solved whether the same reaction occurs *in vivo*. However, even if it occurs, the radical **10** should be less reactive than active oxygen species, because the spin population of **10** is also delocalized as in the case of structure **4**. Therefore, it can be concluded that the highly potent antioxidative activity of **1** (MCI-186) arises from the spin delocalization of its radical intermediate.

The above argument was focused on the reactions in the aqueous medium. It could be also applied to the reaction in the lipid phase without major revision, because the calculated spin densities are essentially the same among gaseous phase, aqueous phase, and hydrogen bonded complex (Table 6). For example, the values for O6 of **4** are 0.330, 0.314, and 0.304 for the gas phase, aqueous phases, and hydrogen-bonded complex, respectively. One different point between the lipid- and aqueous-phase reactions may be present in the first radical-scavenging reaction. After intravenous injection, **4** first stays in the physiological solution of pH 6.8−7.4. Then, the anionic and neutral form of **1** should be equally populated, because the pK_a of **1** is about 7. In such an aqueous medium, the anionic form preferentially reacts with active oxygen species occurring in intra- and extracellular regions, resulting in the production of **3**. However, in the lipid phase the anionic form is not stable; thus the radical intermediate **3** would be produced by direct hydrogen abstraction reaction from the neutral form.

Combining the present calculated data for hyperfine coupling constants with the corresponding ESR experimental data, it is reasonable to say that H10 of **4** is an exchangeable proton. This is a chemically interesting finding, because H10 is the hydrogen atom attached to carbon, C4. **4** should thus be equilibrated with the anionic radical **4′** at body temperature. As shown in Table 6, spin population is more largely delocalized in **4′** than in **4** itself. In the aqueous medium, the spin population on O6 decreases on going from **4** to **4′** , whereas those on both N2 and C4 largely increases. Therefore, the occurrence of **4′** should contribute greatly to the antioxidative ability of **2** (or **1**) at least at body temperature in the aqueous medium.

Finally, it is of great interest to compare the electronic structure of **4** with those of the radical states of naturally occurring antioxidative reagents such as vitamins C and E. Abe et al.[32] have studied the reaction between L-ascorbic acid (vitamin C) and •OH using ab initio and semiempirical molecular orbital calculations. According to their results, a key intermediate radical (ascorbate anion radical; **17** in the reference) is produced, and its spin population was shown to be delocalized on the ring and oxygen atoms. Burton et al.[33] have studied H atom abstraction by peroxyl radicals from α -tocopherol (vitamin E). It was suggested that the activity of α-tocopherol is due to the stabilization of the chromanoxyl radical, that is, (i) the extent of orbital overlap between the 2p type lone pair on the para oxygen atom and the aromatic π electron system, and (ii) the electron-donating or -withdrawing, character of the group bonded to the para oxygen atom. Therefore, the spin delocalization in the radical state seems to be a shared property among most of the highly potent antioxidative agents.

Conclusions

In this work, the radical reaction of **1** was investigated by using its model molecule **2**. **4** was shown to be a stable radical intermediate in the aqueous medium. It was evidenced that all of the radical intermediates occurring in the reaction of **2**, such as **4**, **4′**, and **10**, have highly delocalized spin population. Combining these results with the data for their SOMO levels, such radical species exhibit less reactivity as an oxidant than typical active oxygen species, •OH and LOO• radicals. Therefore, **1** (MCI-186) should play a significant role in inhibiting lipid peroxidation.

Acknowledgment. The major part of the present calculation was carried out using the Cray C916/12256 super computer system of the information processing center of Tokyo Institute of Technology. The authors wish to thank the center of our institute for allotment of CPU time. The calculation was

partially carried out using computer systems of the Institute for Molecular Science (IMS), Okazaki, Japan. We also wish to thank IMS.

References and Notes

(1) Flamm, E. S.; Demopoulos, H. B.; Seligman, M. L.; Poser, R. G.; Ransohoff, J. *Stroke*, **1978**, *9*, 445.

(2) McCord, J. M. N. *Engl. J. Med.* **1985**, *312*, 159.

(3) Abe, K.; Yuki, S.; Kogure, K. *Stroke* **1988**, *19*, 480.

(4) Nishi, H.; Watanabe, T.; Sakurai, H.; Yuki, S.; Ishibashi, A. *Stroke* **1989**, *20*, 1236.

(5) Watanabe, T.; Yuki, S.; Egawa, M.; Nishi, H. *J. Pharmacol. Exp. Ther.* **1994**, *268*, 1597.

(6) Elguero, J.; Marzin, C.; Katritzky, A. R.; Linda, P. *The Tautomerism Of Heterocycles*; Academic Press: New York, 1976.

(7) Elguero, J. Comprehensive Heterocyclic Chemistry; Rees, C. W., Katrizky, A. R., Eds.; Pergamon: Oxford, 1984; Vol. 5.

(8) Freyer, W.; Köppel, H.; Radeglia, R.; Malewski, G. *J. Prakt. Chem.* **1983**, *325*, 238.

(9) Barone, V.; Adamo, C. *J. Phys. Chem.* **1995**, *99*, 15062.

(10) Florián, J.; Baumruk, V.; Leszczyński, J. *J. Phys. Chem.* **1996**, *100*, 5578.

(11) Matyus, P.; Fuji, K.; Tanaka, K. *Tetrahedron* **1994**, *50*, 2405.

(12) Nowak, M. J.; Kapinski, K.; Kwiatkowski, J. S.; Leszczyński, J. *J. Phys. Chem.* **1996**, *100*, 3527.

(13) Harris, N. J.; Lammertsma, K. *J. Am. Chem. Soc.* **1996**, *118*, 8048.

(14) Ono, S.; Okazaki, K.; Sakurai, M.; Inoue, Y. In Preparation.

(15) Lehmann, F.-M.; Bretz, N.; Bruchhausen, F. V.; Wurm, G. *Biochem. Pharmacol.* **1989**, *38*, 1209.

(16) Omelka, L.; Meske, M.; Schulz, M. *J. Parkt. Chem. Chem.-Ztg.* **1993**, *335*, 435.

(17) Yamamoto, Y.; Kuwahara, T.; Watanabe, K.; Watanabe, K. *Redox Rep.* **1996**, *2*, 333.

(18) Frisch, M. J.; Trucks, G. W.; Schlegel, H. B.; Gill, P. M. W.; Johnson, B. G.; Robb, M. A.; Cheeseman, J. R.; Keith, T.; Petersson, G. A.; Montgomery, J. A.; Raghavachari, K.; Al-Laham, M. A.; Zakrzewski, V. G.; Ortiz, J. V.; Foresman, J. B.; Peng, C. Y.; Ayala, P. Y.; Chen, W.; Wong, M. W.; Andres, J. L.; Replogle, e. S.; Gomperts, R.; Martin, R. L.; Fox, D. J.; Binkley, J. S.; Defrees, D. J.; Baker, J.; Stewart, J. P.; Head-Gordon, M.; Gonzalez, C.; Pople, J. A., *Gaussian 94*, Revision B.1 and Revision B.3; Gaussian Inc.: Pittsburgh, PA, 1995.

(19) Hariharan, P. C.; Pople, J. A. *Theor. Chim. Acta* **1973**, *28*, 213.

(20) Becke, A. D. *J. Chem. Phys.* **1993**, *98*, 5648.

(21) Barone, V. Structure, Magnetic Properties and Reactivities of Open-Shell Species from Density Functional and Self-Consistent Hybrid. In *Recent Advances in Density Functional Methods, Part 1*; Chong, D. P., Ed.; Recent Advances in Computational Chemistry-Vol. 1; World Scientific Publishing: Singapore, 1995.

(22) Barone, V.; Adamo, C.; Russo, N. *Int. J. Quantum Chem.* **1994**, *52*, 963.

(23) Barone, V.; Adamo, C.; Russo, N. *Chem. Phys. Lett.* **1993**, *212*, 5.

(24) Adamo, C.; Barone, V.; Fortunelli, A. *J. Chem. Phys.* **1995**, *102*, 384.

(25) Barone, V. *Theor. Chim. Acta* **1995**, *91*, 113.

(26) Barone, V. *Chem. Phys. Lett.* **1996**, *262*, 201.

(27) Shohoji, M. C. B. L.; Novais, H. M.; Vieira, A. J. S. C. *J. Chem. Soc., Perkin Trans. 2* **1995**, 2101.

(28) Ono, S.; Okazaki, K.; Sakurai, M.; Inoue, Y. In preparation.

(29) Jovanovic, S. V.; Neta, P.; Simic, M. G. *Mol. Pharm.* **1985**, *28*, 377.

(30) Sevilla, M. D.; Neta, P.; Marnett, L. J. *Biochem. Biophys. Res. Commun.* **1983**, *115*, 800.

(31) Uri, N. Autoxidation and Antioxidant. In *Autoxidation and Antioxidant*; Lundberg, W. O., Ed.; John Wiley & Sons: New York, 1961; Vol. I, Chapter 4.

(32) Abe, Y.; Okada, S.; Nakao, R.; Horii, T.; Inoue, H.; Taniguchi, S.; Yamabe, S. *J. Chem. Soc., Perkin Trans 2* **1992**, 2221.

(33) Burton, G. W.; Doba, T.; Gabe, E. J.; Hughes, L.; Lee, F. L.; Prasad, L.; Ingold, K. U. *J. Am. Chem. Soc.* **1985**, *107*, 7053.